

Optimal harvesting and spatial patterns in a semi arid vegetation system

Hannes Uecker

Institut für Mathematik, Universität Oldenburg,
D26111 Oldenburg, hannes.uecker@uni-oldenburg.de

January 12, 2016

Abstract

We consider an infinite time horizon spatially distributed optimal harvesting problem for a vegetation and soil water reaction diffusion system, with rainfall as the main external parameter. By Pontryagin's maximum principle we derive the associated four component canonical system, and numerically analyze this and hence the optimal control problem in two steps. First we numerically compute a rather rich bifurcation structure of *flat* (spatially homogeneous) and *patterned* canonical steady states (FCSS and PCSS, respectively), in 1D and 2D. Then we compute time dependent solutions of the canonical system that connect to some FCSS or PCSS. The method is efficient in dealing with non-unique canonical steady states, and thus also with multiple local maxima of the objective function. It turns out that over wide parameter regimes the FCSS, i.e., spatially uniform harvesting, are not optimal. Instead, controlling the system to a PCSS yields a higher profit. Moreover, compared to (a simple model of) private optimization, the social control gives a higher yield, and vegetation survives for much lower rainfall. In addition, the computation of the optimal (social) control gives an optimal tax to incorporate into the private optimization.

Keywords: distributed optimal control, bioeconomics, optimal harvesting

MSC: 49J20, 49N90, 35B32

1 Introduction and main results

Vegetation patterns such as spots and stripes appear in ecosystems all over the world, in particular in so called semi arid areas [DBC⁺08]. Semi arid here means that there is enough water to support *some* vegetation, but not enough water for a dense homogeneous vegetation. Such systems are often modeled in the form of two or more component reaction–diffusion systems for plant and water densities, with rainfall R as the main bifurcation parameter, and the patterns are attributed to a positive feedback loop between plant density and water infiltration. Starting with a homogeneous equilibrium of high plant density for large R , stationary spatial patterns appear as R is lowered, often following a universal sequence [GRS14]. This may lead to catastrophic, sometimes irreversible, regime shifts, where a patterned vegetation

suddenly dies out completely, leaving a desert behind as R drops below a certain threshold, or as some other parameter such as harvesting or grazing by herbivores is varied. There is a rather large number of specific models, each agreeing with field observations in various parameter regimes, see e.g., [SZvHM01, HRvdB⁺01], and [RDdRvdK04] for a review, or [SBB⁺09, ZKY⁺13] and the references therein for further reviews including more recent work on early warning signals for desertification and other critical transitions, usually associated with subcritical bifurcations.

A so far much less studied problem is the spatially distributed dynamic optimal control (OC) of vegetation systems by choosing harvesting or grazing by herbivores in such a space and time dependent way that some economic objective function is maximized. Following [BX10] we consider an infinite time horizon OC problem for a reaction–diffusion system for vegetation biomass and soil water, which is roughly based on [HRvdB⁺01]. Related optimal control problems have also been considered in [BX08, Xep10, BEGX13], with the focus on the so called “Optimal Diffusion Instability” of flat canonical steady states (FCSS, see §1.1 for OC related definitions), which similar to a Turing bifurcation yields the bifurcation of spatially *patterned* canonical steady states (PCSS) from FCSS. However, in these works, and in [BX10], only few PCSS have been actually calculated numerically, and no canonical paths, i.e., time dependent solutions of the canonical system. Finite time horizon cases recently have been considered in [CPB12, ACKLT13, ADS14], mostly focusing on theoretical aspects, and on problems with control constraints, which altogether gives a rather different setting than ours; see also Remark 1.3.

Here we apply the numerical framework from [GU15, Uec15] to the so called canonical system for the states and co–states, derived via Pontryagin’s Maximum Principle. First we calculate (branches) of canonical steady states (CSS), including branches of PCSS, and in a second step canonical paths connecting to some CSS. Our main result is that in wide ranges of parameters, in particular for low rainfall R , FCSS and their canonical paths are not optimal, and that controlling the system to a PCSS yield a higher profit than uniform harvesting. Thus, this seems to be the first example of a bio-economically motivated optimal control problem, where the global bifurcation structure of CSS has been computed in some detail, showing multiple CSS at fixed parameter values and with dominant non–spatially homogeneous steady states, and where moreover canonical paths to such PCSS have been computed, with significant gains in welfare. We also compare these results to results for the same system with (initially) no external control, i.e., the system with private optimization, and find that the optimal control significantly increases the profit, and supports vegetation at significantly lower rainfall levels, which again has important welfare implications. Remarkably, in our system the co-state of the vegetation can be identified with a tax for the private optimization problem, and thus, by solving the canonical system we find an optimal space and time dependent tax for the private optimization problem.

A standard reference on ecological economics or “Bioeconomics” is [Cla90], including a very readable account, and applications, of Pontryagin’s Maximum Principle in the context of ODE models; see also [LW07]. A review of management rules for semi arid grazing systems including comparison to real data, and making plain the importance of such rules, is given in

[QB12]. However, the (family of) models discussed there consist of discrete time evolutions without spatial dependence, and with focus on the rainfall R as a time-dependent stochastic parameter; here we consider a deterministic PDE model. Thus comparison between the two (classes of) models is difficult, but it should be interesting to include spatial dependence into the model in [QB12].

Finally, in, e.g., [Neu03], [DL09], stationary spatial OC problems for a fishery model are considered, including numerical simulations, which correspond to our calculation of canonical steady states for our model (3) below. The results of [Neu03, DL09] show that for their models it is *economically optimal* to provide “no-take” marine reserves. This is similar to our finding of *optimal* patterned canonical steady states, but here we go beyond the steady case with the computation of optimal paths. This in particular tells us how to dynamically control the system to an (at least locally) optimal steady state. Moreover, even for the steady states there are important technical differences between the OC problems considered in [Neu03, DL09] with *unique* positive canonical steady states, and the OC problems considered here, which in relevant parameter regimes are distinguished by having *many* canonical steady states, of which several can be locally stable (see Remark 1.2 for definitions, and, again, Remark 1.3.) Thus, management rules for our system are considerably more complicated than those in, e.g., [Neu03, DL09], as they must take the different CSS into account, and given an initial state, must decide to the domain of attraction of which CSS it belongs. Partly to illustrate this point, we also compute a Skiba (or indifference) point [Ski78] between different CSS in §2.3.2.

In the remainder of this Introduction we explain the model and the use of Pontryagin’s Maximum Principle to derive the canonical system (§1.1), explain the basic idea of the numerical method (§1.2), and summarize the results (§1.3). In §2 we present the quantitative results, and in §3 we give a brief further discussion. The method has been implemented in `Matlab` as an “add-on” package `p2pOC` to the continuation and bifurcation software `pde2path` [UWR14], and the `matlab` functions and scripts to run (most of) the simulations, the underlying libraries, manuals of the software, and some more demos can be downloaded at [Uec14].

Acknowledgment. I thank D. Graß, ORCOS Wien, for valuable comments on the economic terminology, and the anonymous referees for valuable questions and comments on the first version of the manuscript.

1.1 Problem setup

In dimensionless variables the model for vegetation and soil water with social optimization from [BX10] is as follows. Let $\Omega \subset \mathbb{R}^d$ be a one-dimensional (1D) or two-dimensional (2D) bounded domain, $v = v(x, t)$ the vegetation density at time $t \geq 0$ and space $x \in \Omega$, $w = w(x, t)$ the soil water saturation,

$E = E(x, t)$ the harvesting effort (control), $H(v, E) = v^\alpha E^{1-\alpha}$ the harvest, and

$$J(v_0, w_0, E) = \frac{1}{|\Omega|} \int_0^\infty e^{-\rho t} \int_\Omega J_c(v(x, t), E(x, t)) \, dx \, dt \quad (1)$$

the (spatially averaged) objective function, where $\rho > 0$ is the discount rate, and

$$J_c(v, E) = pH(v, E) - cE \quad (2)$$

is the (local) current value profit. This profit depends on the price p , the costs c for harvesting, and v, E in a classical Cobb–Douglas form with elasticity parameter $0 < \alpha < 1$. The problem reads

$$V(v_0, w_0) = \max_{E(\cdot, \cdot)} J(v_0, w_0, E), \quad \text{where} \quad (3a)$$

$$\partial_t v = d_1 \Delta v + [g w v^\eta - d(1 + \delta v)]v - H(v, E), \quad (3b)$$

$$\partial_t w = d_2 \Delta w + R(\beta + \xi v) - (r_u v + r_w)w, \quad (3c)$$

$$(v, w)|_{t=0} = (v_0, w_0). \quad (3d)$$

The parameters and default values are explained in Table 1, together with brief comments on the terms appearing in (3). One essential feature of (3b,c) is the positive feedback loop between vegetation v and water w . Clearly, the vegetation growth rate $g w v^\eta$ increases with w , but the vegetation v also has a positive effect on water infiltration, for instance due to loosened soil, modeled by $R\xi v$ in (3c).

Remark 1.1. In [BX10], E is also referred to as the grazing by herbivores, and (3) is called a semi arid grazing system. This seems somewhat oversimplified, because from a practical point of view, controlling in detail the movement and grazing behavior of, e.g., cattle, certainly is a more complicated problem than controlling genuine harvesting. Thus, henceforth we stick to calling E the harvesting effort.]

We complement (3) with homogeneous Neumann boundary conditions (BC) $\partial_\nu v = 0$ and $\partial_\nu w = 0$ on $\partial\Omega$, where ν is the outer normal. The discounted time integral in (1) is typical for economic (here bioeconomic) problems, where “profits now” weight more than mid or far future profits. More specifically, ρ corresponds to a long-term investment rate. We normalize J_{ca} by $|\Omega|$ for easier comparison between different domains and space dimensions. In (bio)economics, the control E , chosen externally by a “social planner” to maximize the social value J , is often called social control, as opposed to private optimization, see (19) below. Finally, the max in (3a) runs over all *admissible* controls E ; essentially this means that $E \in L^\infty([0, \infty) \times \Omega, \mathbb{R})$, where moreover implicitly we have the control constraint $E \geq 0$, and state constraint $v, w \geq 0$ for the associated solutions of (3b,c). However, in our simulations these constraints will always naturally be fulfilled, i.e., *inactive*, see also Remark 1.3.

Introducing the costates $(\lambda, \mu) = (\lambda, \mu)(x, t)$ and the (local current value) Hamiltonian

$$\begin{aligned} \mathcal{H}(v, w, \lambda, \mu, E) = & J_c(v, E) + \lambda [d_1 \Delta v + (g w v^\eta - d(1 + \delta v))v - H] \\ & + \mu [d_2 \Delta w + R(\beta + \xi v) - (r_u v + r_w)w], \end{aligned} \quad (4)$$

by Pontryagin’s Maximum Principle for $\tilde{\mathcal{H}} = \int_0^\infty e^{-\rho t} \overline{\mathcal{H}}(t) dt$ with the spatial integral

$$\overline{\mathcal{H}}(t) = \int_\Omega \mathcal{H}(v(x, t), w(x, t), \lambda(x, t), \mu(x, t), E(x, t)) dx, \quad (5)$$

param.	meaning	default values
g, η	coefficient and exponent in plant growth rate $g w v^\eta$	$g = 0.001, \eta = 0.5$
d, δ	coefficients in plant death rate $d(1 + \delta v)$	$d = 0.03, \delta = 0.005$
β, ξ	coefficients in the infiltration function $\beta + \xi v$,	$\beta = 0.9, \xi = 0.001$
R	rainfall parameter, used as main bifurcation parameter	between 4 and 100
r_u, r_w	water uptake and evaporation parameters in the water loss rate $r_u v + r_w$	$r_u = 0.01, r_w = 0.1$
$d_{1,2}$	diffusion constants for vegetation and water (resp.)	$d_1 = 0.05, d_2 = 10$
ρ	discount rate	$\rho = 0.03$
c, p, α	(economic) param. in the harvesting $H(v, E) = v^\alpha E^{1-\alpha}$ and in the value $J_c(v, E) = p H(v, E) - c E$ (ρ and p used as bifurcation param. in §2.5)	$c = 1, p = 1.1, \alpha = 0.3$

Table 1: Dimensionless parameters and default values in (3); see [BX10] for further comments on the modeling. In particular, following [BX10, §4.2] we have a rather larger d_2 .

an optimal solution (v, w, λ, μ) has to solve the canonical system (CS)

$$\partial_t v = \partial_\lambda \mathcal{H} = d_1 \Delta v + [g w v^\eta - d(1 + \delta v)]v - H, \quad (6a)$$

$$\partial_t w = \partial_\mu \mathcal{H} = d_2 \Delta w + R(\beta + \xi v) - (r_u v + r_w)w, \quad (6b)$$

$$\begin{aligned} \partial_t \lambda = \rho \lambda - \partial_v \mathcal{H} = \rho \lambda - p \alpha v^{\alpha-1} E^{1-\alpha} - \lambda [g(\eta + 1) w v^\eta - 2d\delta v - d - \alpha v^{\alpha-1} E^{1-\alpha}] \\ - \mu (R\xi - r_u w) - d_1 \Delta \lambda, \end{aligned} \quad (6c)$$

$$\partial_t \mu = \rho \mu - \partial_w \mathcal{H} = \rho \mu - \lambda g v^{\eta+1} + \mu (r_u v + r_w) - d_2 \Delta \mu, \quad (6d)$$

where $E = \arg\max_{\tilde{E}} \mathcal{H}(v, w, \lambda, \mu, \tilde{E})$, which is obtained from solving $\partial_E \mathcal{H} = 0$ for E , giving

$$E = \left(\frac{(p - \lambda)(1 - \alpha)}{c} \right)^{1/\alpha} v. \quad (6e)$$

The costates (λ, μ) also fulfill zero flux BC, and derivatives like $\partial_v \mathcal{H}$ etc are taken variationally, i.e., for $\overline{\mathcal{H}}$. For instance, for $\Phi(v, \lambda) = \lambda \Delta v$ we have $\overline{\Phi}(v, \lambda) = \int_\Omega \lambda \Delta v \, dx = \int_\Omega (\Delta \lambda) v \, dx$ by Gauß' theorem, hence $\delta_v \overline{\Phi}(v, \lambda)[h] = \int (\Delta \lambda) h \, dx$, and by the Riesz representation theorem we identify $\delta_v \overline{\Phi}(v, \lambda)$ and hence $\partial_v \Phi(v, \lambda)$ with the multiplier $\Delta \lambda$. Moreover, we used the so called intertemporal transversality conditions

$$\lim_{t \rightarrow \infty} e^{-\rho t} \int_\Omega v(x, t) \lambda(x, t) \, dx = 0 \text{ and } \lim_{t \rightarrow \infty} e^{-\rho t} \int_\Omega w(x, t) \mu(x, t) \, dx = 0, \quad (6f)$$

which is justified since we are only interested in bounded solutions.

For convenience setting

$$u := (v, w, \lambda, \mu) : \Omega \times [0, \infty) \rightarrow \mathbb{R}^4, \quad (7)$$

we collect (6a–e) and the boundary conditions into

$$\partial_t u = -G(u) := \mathcal{D}\Delta u + f(u), \quad \mathcal{D} = \begin{pmatrix} d_1 & 0 & 0 & 0 \\ 0 & d_2 & 0 & 0 \\ 0 & 0 & -d_1 & 0 \\ 0 & 0 & 0 & -d_2 \end{pmatrix}, \quad (8a)$$

$$\partial_\nu u = 0 \text{ on } \partial\Omega, \quad (v, w)|_{t=0} = (v_0, w_0). \quad (8b)$$

In (8b) we only have initial conditions for the states, i.e., half the variables, and (8a) is ill-posed as an initial value problem due to the backward diffusion in (λ, μ) . Thus, below we shall further restrict the transversality condition (6f) to requiring that $u(t)$ converges to a steady state, i.e. a solution of

$$G(u) = 0, \quad \partial_\nu u = 0 \text{ on } \partial\Omega. \quad (9)$$

Remark 1.2. (Definitions and notations) A solution u of the canonical system (8) is called a *canonical path*, and a solution \hat{u} of (9) is called a *canonical steady state (CSS)*. With a slight abuse of notation we also call (v, w, E) with E given by (6e) a canonical path, suppressing the associated co-states λ, μ . In particular, if \hat{u} is a CSS, so is $(\hat{v}, \hat{w}, \hat{E})$. A CSS \hat{u} is called *flat* if it is spatially homogeneous, and *patterned* otherwise, and we use the acronyms FCSS and PCSS, respectively. For convenience, given $t \mapsto u(t)$ we also write

$$J(u) := J(v_0, w_0, E), \quad (10)$$

with (v_0, w_0) and E (via (6e)) taken from u . A canonical path u (or (v, w, E)) is called *optimal* if there is no canonical path starting at the state values $(v(0), w(0))$ and yielding a higher J than $J(u)$. As a special case, a CSS $\hat{u} = (\hat{v}, \hat{w}, \hat{\lambda}, \hat{\mu})$ is called optimal if there is no canonical path starting at (\hat{v}, \hat{w}) and yielding a higher J than $J(\hat{v}, \hat{w}, \hat{E})$. We use the acronyms OSS for any optimal CSS, and FOSS and POSS for optimal flat or patterned CSS \hat{u} , respectively. An OSS \hat{u} is called *locally stable* if for all admissible (v_0, w_0) close to (\hat{v}, \hat{w}) there is an optimal path u with $\lim_{t \rightarrow \infty} u(t) = \hat{u}$.¹ Similarly, \hat{u} is called *globally stable* if for all admissible (v_0, w_0) the associated optimal path has $\lim_{t \rightarrow \infty} u(t) = \hat{u}$. Finally, the *domain of attraction* of a locally (or globally) stable OSS \hat{u} is defined as the set of all (v_0, w_0) such that the associated optimal path u fulfills $\lim_{t \rightarrow \infty} u(t) = \hat{u}$. See also [GU15] for more formal definitions, and further comments on the notion of optimal system, and, e.g., the transversality condition (6f).]

Remark 1.3. For background on OC in a PDE setting see for instance [Trö10] and the references therein, or specifically [RZ99a, RZ99b, LM01] and [AAC11, Chapter5] for Pontryagin’s Maximum Principle for OC problems for semilinear parabolic state evolutions. However, these works are in a finite time horizon setting, often the objective function is linear in the

¹For “close to” and lim we may use, e.g., the $H^1(\Omega)$ norm, but since all solutions will be smooth, for instance as solutions of semilinear elliptic systems with smooth coefficients, we decided to omit the introduction of function spaces here. Similarly, (v_0, w_0) “admissible” should be read as $v_0(x), w_0(x) \geq 0$ for $x \in \Omega$.

control, and there are state or control constraints. For instance, denoting the control by $k = k(x, t)$, often k is chosen from some bounded interval K , and therefore is not obtained from the analogue of (6e), but rather takes values from ∂K , which is usually called bang-bang control. In, e.g., [CPB12, ACKLT13], some specific models of this type have been studied in a rather theoretical way, i.e., the focus is on deriving the canonical system and showing well-posedness and the existence of an optimal control. [ADS14] additionally contains numerical simulations for a finite time horizon control-constrained OC problem for a three species spatial predator-prey system, again leading to bang-bang type controls. See also [NPS11] and the references therein for numerical methods for (finite time horizon) constrained parabolic optimal control problems.

Similarly, the (stationary) fishery problems in [Neu03, DL09] come with harvesting (i.e. control) constraints. Moreover, in contrast to our zero-flux boundary conditions (8b) Dirichlet boundary conditions are imposed. In [KXL15] the models from [Neu03, DL09] are extended to Robin boundary conditions, and a finite time horizon, with a discounted profit of the form $J = \int_0^T \int_{\Omega} p e^{-\rho t} h(x, t) u(x, t) dx dt$, where $p, \rho > 0$ denote the price and discount rate, h is the harvest, and u the (fish) population density, which fulfills a rather general semilinear parabolic equation including advection. The first focus is again on well-posedness and the first order optimality conditions, and numerical simulations are presented for some specific model choices, illustrating the dynamic formation and evolution of marine reserves. However, the setting again is quite different from ours, due to the finite time horizon, and since J is linear in h and u , and since consequently there are constraints on h , leading to (unique) bang-bang controls.

Here we do not consider (active) control or state constraints, and no terminal time, but the infinite time horizon. Our models and method are motivated by [BX08, BX10], which also discuss Pontryagin’s Maximum Principle in this setting. We do not aim at theoretical results, but rather consider (8) after a spatial discretization as a (large) ODE problem, and essentially treat this using the notations and ideas from [BPS01] and [GCF⁺08, Chapter 7], and the algorithms from [GU15, Uec15], to numerically compute optimal paths.]

1.2 Solution steps

Using the canonical system (8) we proceed in two steps: first we compute (branches of) CSS, and second we solve the “connecting orbit problem” of computing canonical paths connecting to some CSS. Thus we take a broader perspective than aiming at computing just one optimal control, given an initial condition (v_0, w_0) , which without further information is an ill-posed problem anyway. Instead, our method aims to give a somewhat global picture by identifying the (in general multiple) optimal CSS and their respective domains of attraction, as follows:

- (i) To calculate CSS (which automatically fulfill (6f)) we set up (9) as a bifurcation problem and use the package `pde2path` [UWR14, DRUW14] to find a branch of FCSS, from which various branches of PCSS bifurcate. We focus on the rainfall parameter R as the main bifurcation parameter, but in §2.5 also briefly discuss the dependence on the discount rate ρ and the price p as bifurcation parameters. By calculating in parallel

the (spatially averaged) current value profits

$$J_{c,a}(v, E) := \frac{1}{|\Omega|} \int_{\Omega} J_c(v(x), E(x)) \, dx \quad (11)$$

of the CSS we can moreover immediately find which of the CSS maximize $J_{c,a}$ and hence $J = J_{c,a}/\rho$ amongst the CSS.

- (ii) In a second step we calculate canonical paths ending at a CSS (and often starting at the state values of a different CSS), and the objective values of the canonical paths.

Using a Finite Element Method (FEM) discretization, (8) is converted into the ODE system (with a slight abuse of notation)

$$M \frac{d}{dt} u = -G(u), \quad (12)$$

where $u \in \mathbb{R}^{4n}$ is a large vector containing the nodal values of $u = (v, w, \lambda, \mu)$ at the n spatial discretization points (typical values are $n = 30$ to $n = 100$ in 1D, and $n = 1000$ and larger in 2D), and $M \in \mathbb{R}^{4n \times 4n}$ is the so called mass matrix, which is large but sparse. In (12) and the following we mostly suppress the dependence of G on the rainfall R (or the other parameters). For (i) we thus need to solve the problem $G(u) = 0$, which can be considered as an elliptic problem after changing the signs in the equations $G_{3,4}(u) = 0$ for the costates.

For (ii) we choose a suitable truncation time $T > 0$ and replace the transversality condition (6f) by the condition

$$u(T) \in W_s(\hat{u}) \text{ and } \|u(T) - \hat{u}\| \text{ small}, \quad (13)$$

where $W_s(\hat{u})$ is the stable manifold of the CSS \hat{u} for the finite dimensional approximation (12) of (6). In practice we use

$$u(T) \in E_s(\hat{u}) \text{ and } \|u(T) - \hat{u}\| \text{ small}, \quad (14)$$

where $E_s(\hat{u})$ is the stable eigenspace of \hat{u} , i.e., the linear approximation of $W_s(\hat{u})$ at \hat{u} . At $t = 0$ we already have the boundary conditions

$$(v, w)|_{t=0} = (v_0, w_0) \in \mathbb{R}^{2n} \quad (15)$$

for the states. To have a well-defined two point boundary value problem in time we thus need

$$\dim E_s(\hat{u}) = 2n. \quad (16)$$

Since the (generalized, in the sense of M on the left hand side of (12)) eigenvalues of the linearization $-\partial_u G(\hat{u})$ of (8) around \hat{u} are always symmetric around $\rho/2$, see [GU15, Appendix A], we always have $\dim E_s(\hat{u}) \leq 2n$. The number

$$d(\hat{u}) = 2n - \dim E_s(\hat{u}) \quad (17)$$

is called the *defect* of \hat{u} , a CSS \hat{u} with $d(\hat{u}) > 0$ is called *defective*, and if $d(\hat{u}) = 0$, then \hat{u} has the so called *saddle point property* (SPP). Clearly, these are the only CSS such that for all (v_0, w_0) close to (\hat{v}, \hat{w}) we may expect a solution for the connecting orbits problem

$$M \frac{d}{dt} u = -G(u), \quad (v, w)|_{t=0} = (v_0, w_0), \quad u(T) \in E_s(\hat{u}), \text{ and } \|u(T) - \hat{u}\| \text{ small}. \quad (18)$$

See [GU15] for further comments on the significance of the SPP (16) on the discrete level, and its (mesh-independent) meaning for the canonical system as a PDE.

1.3 Results

The bifurcation diagram (i) for (9) turns out to be quite rich, already over small 1D domains. Thus we mostly focus on 1D, but we include a short 2D discussion in §2.4. Details will be given in §2, but in a nutshell we have: In pertinent R regimes there are many CSS, but most of them do not fulfill the SPP, and most of these that do fulfill the SPP are not optimal. On the other hand, in particular at low R there are locally stable POSS (patterned optimal steady states). Before further commenting on this, we briefly review results for the so called uncontrolled case.

In [BX10, §2] it is shown that the case of private objectives, where economic agents (ranchers) are located at each site x , and each one maximizes his or her private profits, leads to the system

$$\partial_t v = d_1 \Delta v + (g w v^\eta - d(1 + \delta v) - A)v, \quad (19a)$$

$$\partial_t w = d_2 \Delta w + R(\beta + \xi v) - (r_u v + r_w)w, \quad (19b)$$

i.e., the harvest is $H = Av$, $A > 0$ a fixed parameter. In detail, ranchers with certain property rights individually maximizing $\pi(v, E) = p v^\alpha E^{1-\alpha} - cE$ leads to

$$E = \gamma v \text{ with } \gamma = \left(\frac{p(1-\alpha)}{c} \right)^{1/\alpha} \text{ and hence } A = \gamma^{1-\alpha}. \quad (20)$$

The same happens in the so called open access case, where agents may harvest freely, giving $E = \hat{\gamma} v$ with $\hat{\gamma} = \left(\frac{c}{p} \right)^{-1/\alpha}$ and hence $A = \hat{\gamma}^{1-\alpha}$. On the other hand, (19) can also be seen as a “undisturbed Nature” case with modified vegetation death rates $\tilde{d} = d + A$ and $\tilde{\delta} = \frac{d}{d+A}$. For the economic parameters $(c, p, \alpha) = (1, 1.1, 0.3)$ from Table 1 we obtain $A = 0.543$, which is rather large compared to the original $d = 0.03$ from Table 1.

The bifurcation picture for steady states of (19) is roughly similar to that of (9), but there are also significant differences, and we altogether summarize our results as follows:

- (a) For large R there is a “high vegetation” FCSS, which is a globally stable FOSS (flat optimal steady state).
- (b) For smaller R the FCSS from (a) loses optimality, and there bifurcate branches of (locally stable) POSS (Patterned Optimal Steady States). In particular, we can calculate canonical paths from the state values of the FCSS to some POSS which increase the profit (up to 40%, see 32).
- (c) The uncontrolled flat steady states (FSS) of (19) only exist for much larger R values than the FCSS. At equal R , the profit J (or equivalently the discounted value J/ρ) of the FSS is much lower (e.g., one tenth, see Table 2, bottom center) than the value of the FCSS of (9).
- (d) For the initial value problem (19) we may consider the stability of steady states, while CSS at best have the SPP. It turns out that the FSS branch loses stability at a much larger value of R to a patterned steady state of (19), than the FOSS loses optimality in the optimal control problem (3). Thus, in the uncontrolled problem pattern formation sets in at larger R .

Roughly speaking, **(b)** means that at low R it is advantageous to restrict harvesting to certain areas. This is similar to the marine reserves in the fishery models in [Neu03, DL09], and not entirely surprising, as it is well known both in models and in field studies of semi arid systems that also in uncontrolled systems low rainfall levels lead to patterned (or patchy) vegetation, which often can be sustained at lower rainfall levels than a uniform state [SZvHM01, RDdRvdK04, ZKY⁺13]; this is precisely what happens here as well. However, the quantitative differences between steady states of (8) and (19) are quite significant, in particular in the sense **(c),(d)**: The controlled system sustains vegetation at much lower R values, and at equal R it yields a much higher profit than (19). Moreover, the computation of canonical paths from some initial state (often a CSS) to some OSS yields precise information *how* to go to the OSS to maximize the objective function.

Remark 1.4. In economics, the co-states λ and μ are also called *shadow prices*, which are sometimes difficult to interpret; here, however, the shadow price λ has a nice interpretation as an optimal tax for private optimization, as follows. Introducing a tax τ per unit harvest, i.e., setting

$$\tilde{\pi}(v, E) = (p - \tau)v^\alpha E^{1-\alpha} - cE, \quad (21)$$

we obtain

$$E = \left(\frac{(p - \tau)(1 - \alpha)}{c} \right)^{1/\alpha} v \quad (22)$$

instead of (20). Thus, after solving the optimization problem (3) via Pontryagin’s Maximum Principle, and thus in particular computing the shadow prize λ of the vegetation constraint along an optimal path, comparing (22) to (6e) we see that private optimization maximizes J from (1), if the tax τ is set in an in general time and space dependent way as $\tau = \lambda$. $\quad \rfloor$

As already said, our method follows [GU15], where we study optimal controls for a model of a shallow lake ecology/economy, given by a scalar parabolic PDE. However, the results are rather different. First of all, without control, i.e., for a fixed control equal to some parameter, the scalar PDE in [GU15] shows no pattern formation: the patterns in [GU15] are only due to the control, which may be called “control induced pattern formation” or, as in [BX08, BX10], “optimal diffusion instability” (ODI). However, the parameters in [GU15] have to be carefully fine-tuned to obtain POSS, which moreover are only locally stable, see also [Gra15]. Here, to obtain POSS we need no fine-tuning of parameters.

From the methodical and algorithmic point of view, our results for (3) illustrate that our two-step approach is well suited to deal with non-uniqueness of CSS in nonlinear PDE optimal control problems, and the typically associated multiple canonical paths and multiple local maxima of the objective function. See also §3 for further discussion of efficiency.

2 Numerical simulations

2.1 1D canonical steady states bifurcating from the FCSS branch

The bifurcation scenario for the stationary problem $G(u) = 0$ can be studied conveniently with `pde2path`. First we concentrate on the 1D case $u = u(x)$, $x \in (-L, L)$, where the domain length must be chosen in such a way to capture pertinent instabilities of the FCSS branch. In [BX08, BX10] conditions for pattern forming instabilities in terms of the Hamiltonian \mathcal{H} and its derivatives at a FCSS are given. These are similar to the well known Turing space conditions [Mur89], and moreover allow the calculation of the critical wave-number k_c of the bifurcation patterns. For instance, at $R = 5$ [BX10] find $(k_-, k_+) \approx (0.146, 1.455)$ for the band of unstable wave numbers at the FCSS.

If one is interested in accurately capturing the first bifurcation, then one should either fit the domain to the (wave number of the) first instability (see, e.g., [UW14] for examples), or use a very large domain, which gives a rather dense set of allowed wave numbers. However, for simplicity, and with the (expensive) t -dependent canonical paths in mind, here we do not want to use a very large domain, and, moreover, rather take the point of view that the domain comes with the model. Thus, we do not want to be too precise on fitting the domain to the first instability over an infinite domain, and simply choose $L = 5$. Of course, increasing the domain size (certainly in integer multiples of L) will only increase the number of patterns and bifurcations, and on the other hand there is a critical minimal domain size below which no patterns exist.

In order to present our results in a domain independent way we give averaged quantities such as $J_{c,a}$, see (11), and

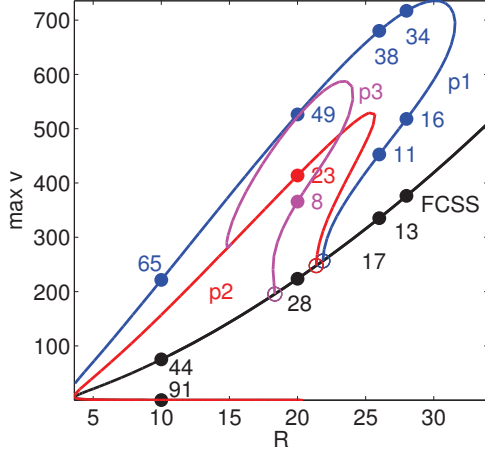
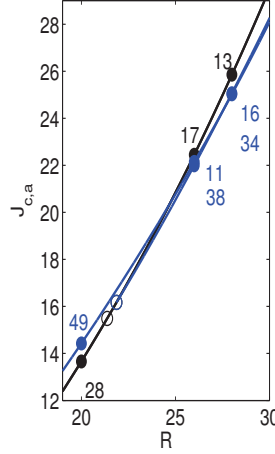
$$\langle v \rangle := \frac{1}{|\Omega|} \int_{\Omega} v(x) dx, \quad \text{and so on.} \quad (23)$$

Figure 1(a) shows a basic bifurcation diagram of 1D CSS. We start with a FCSS at $R = 34$ which can be easily found from an initial guess $(v, w, \lambda, \mu) = (400, 10, 0.5, 1)$ followed by a Newton loop.² See Table 2 for numerical values of some of the FCSS found this way, and of other selected points in the bifurcation diagrams. Following the FCSS branch with decreasing R we find a number of branch points to PCSS, and near $R = 4$ we find a fold for the FCSS branch. The lower FCSS branch continues back to large R , but is not interesting from a modeling point of view. The upper FCSS branch has the SPP until the first bifurcation at $R = R_c \approx 21.5$, where a PCSS branch p1 with period $20/3$ bifurcates subcritically; see the example plots of solutions on p1. This is a pitchfork bifurcation, but here and in general we only follow the branch in one direction; the other direction is often related to the first by symmetry, e.g., spatial translation by half a period.

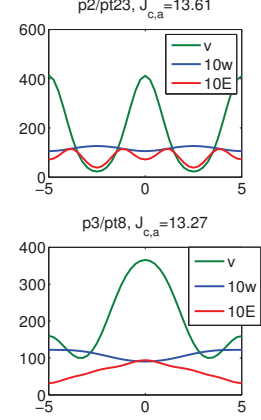
The p1 branch has a fold at $R_f \approx 31$, after which it has the SPP down to a secondary bifurcation at $R_2 \approx 9.4$. Near $R = 3.1$ the p1 branch also has a second fold, after which it continues to larger R as a branch of small amplitude patterns. (a) also shows the PCSS

²(6a,b) also has the trivial solution branch $(v, w) = (0, R\beta/r_w)$, which yields the trivial branch FCSS₀ with $(v, w, \lambda, \mu) = (0, R\beta/r_w, 0, 0)$ (and hence $E = 0$), which however is of little interest here.

(a) partial bifurcation diagram of CSS

(b) $J_{c,a}$ over R 

(c) example CSS plots



(d) example CSS plots, with costates

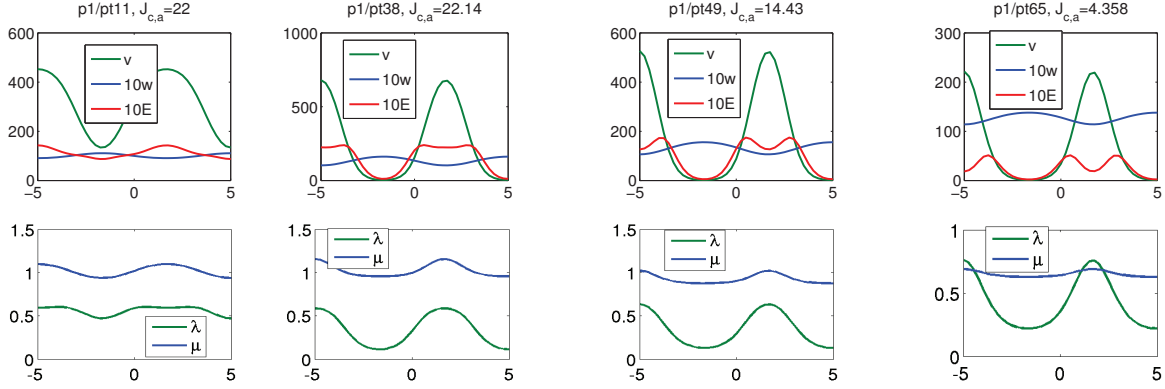


Figure 1: (a) (partial) bifurcation diagram of CSS in 1D, including a (small) selection of bifurcation points indicated by \circ . The labeled points are tabulated in Table 2, and a selection of these solutions together with E (and the co-states for the p1-branch) are plotted in (c),(d). (b) shows the two branches FCSS and p1 with colors as in (a) in a $J_{c,a}$ over R diagram, which allows to identify which CSS maximizes $J_{c,a}$ amongst the CSS (all other branches from (a) have a significantly lower $J_{c,a}$).

branches bifurcating from the second and third bifurcation points on the FCSS; interestingly, p3 connects back to p2 in a secondary bifurcation. However, except for the FCSS branch for $R > R_c$ and the p1 branch between the first fold and the first secondary bifurcation, no other branch has solutions with the SPP, cf. (16).

Figure 1(b) shows the FCSS and p1 branches in a $J_{c,a}$ over R bifurcation diagram. This already shows that at, e.g., $R = 20$ (in fact, for R smaller than about 24.4), solutions on p1 yield a larger $J_{c,a}$ than the FCSS, and thus appear as a candidates for POSS. From the applied point of view, probably the most interesting aspect of the solution plots in (c) and (d) is that after the first fold on the p1 branch the effort E has local minima, not maxima, at the maxima of v . Instead, E has maxima on the slopes near the maximum of v . Taking into account (6e) and the co-state plots in the second row of (d), this can be attributed to the distinctive peaks in λ at the maxima of v . These peaks in the shadow price of the vegetation

point	FCSS/13	p1/16	p1/34	FCSS/17	p1/11	p1/38	FCSS/28	p1/49	p2/23
R	28	28	28	26	26	26	20	20	20
$\langle v \rangle$	376.32	337.92	283.31	335.36	311.63	252.46	223.59	175.49	185.08
$\langle w \rangle$	9.25	10.37	13.17	9.3	10.05	13.34	9.62	13.28	11.64
$\langle \lambda \rangle$	0.59	0.53	0.35	0.59	0.56	0.34	0.62	0.34	0.45
$\langle \mu \rangle$	1.09	1.06	1.06	1.04	1.02	1.03	0.87	0.92	0.89
J_c	25.85	25.06	25.02	22.45	22	22.14	13.66	14.43	13.61
d	0	2	0	0	2	0	2	0	1

point	FCSS/44	FCSS/91	p1/65	FSS*/121	p1*/97	p6*/30	FCSS/105	q1/76	q6/69
R	10	10	10	60	60	60	60	20	20
$\langle v \rangle$	75.08	0.21	71.33	79.73	163.42	86.5	1304.5	183.14	151.22
$\langle w \rangle$	11.46	88.21	12.71	65.51	39.21	61.4	10.06	12.02	14.54
$\langle \lambda \rangle$	0.68	0.9	0.42	NA	NA	NA	0.49	0.35	0.31
$\langle \mu \rangle$	0.5	0.0006	0.65	NA	NA	NA	1.75	0.91	0.91
J_c	3.51	0.002	4.36	14.3	29.31	15.51	120.8	13.93	13.93
d	4	4	0	NA(u)	NA(s)	NA(u)	0	0	0

Table 2: Characteristics of selected points marked in Fig. 1(1D, top half and bottom left in the table), Fig. 2 (bottom center in the table, where * denotes values from the case of private optimization) and Fig. 6 (2D case, bottom right in the table). NA for the * values means that these values are not defined; for the defect the additional u,s are used to indicate unstable vs stable solutions.

evolution illustrate that it is not optimal to harvest at the peaks in v as this will strongly decrease future income. Also note that the (average) shadow prices $\langle \lambda \rangle$ on the p1 branch after the fold are lower than on the FCSS branch at the same R , while at least at low R , $\langle \mu \rangle$ is higher on p1 than on FCSS.

The vegetation patterns (p1 branch) survive for lower R (up to $R_{\text{crit}} \approx 3.1$) than the FCSS branch ($R_{\text{crit}} \approx 3.7$). However, the difference is not large, and this bottom end of R will not be our interest here, despite its significance for critical transitions. Instead, we are interested in the optimality of CSS for intermediate $R_{\text{min}} < R < R_f$, with $R_{\text{min}} = 5$, say.

Remark 2.1. Although our picture of CSS obtained above is already somewhat complicated, naturally it is far from complete. Firstly, we only followed the first three bifurcations from the FCSS branch, and secondly, there are (plenty of) secondary bifurcations on the branches p1, p2 and p3, which here we do not follow. In particular, given that the 1.5-modal (in, e.g., v) branch p1 maximizes J amongst the CSS, a natural question is whether there also exist unimodal or 0.5-modal branches, which might give even higher J . The answer is (partly) yes: while we could not find a 0.5-modal branch, there is a unimodal branch p0, which bifurcates from p2 in a secondary bifurcation, or, more precisely, connects p1 and p2. See §2.5.2 for details, where inter alia we study the bifurcation behavior in the price p . Moreover, p0 then maximizes J amongst the CSS, and, loosely speaking, turns out to be a global maximum for (3).

Nevertheless, until §2.5.2, for the sake of clarity we restrict to the primary branches which bifurcate from the FCSS when varying R . However, one should keep in mind that whatever

method one uses to study optimization problems like (3) it is always possible to be stuck with some local maxima, and to miss some global maximum. \square

2.2 Comparison to private optimization

As already explained in the Introduction, private objectives, i.e., individual ranchers maximizing $\pi(v, E) = pv^\alpha E^{1-\alpha} - cE$, leads to the system

$$\partial_t v = d_1 \Delta v + (g w v^\eta - d(1 + \delta v) - A)v, \quad (24a)$$

$$\partial_t w = d_2 \Delta w + R(\beta + \xi v) - (r_u v + r_w)w, \quad (24b)$$

with $A = \gamma^{1-\alpha} = 0.543$ for the economic parameters $(c, p, \alpha) = (1, 1.1, 0.3)$ from Table 2. In this section we compare the bifurcation diagram in R for steady states of (24), see Fig. 2, to that for (8) in Fig.1.

Roughly speaking, both are similar, but for (24) the bifurcations to patterned steady states occur at larger R , and of course also have to be interpreted differently. First of all, we start the bifurcation diagram at $R = 130$ with a dynamically stable flat steady state (FSS) of (24), which loses stability at $R_c \approx 122$ due to a supercritical pitchfork bifurcation of a branch p1nc of patterns with period 5. There are a number of further bifurcations from the FSS branch; as an example we give p6nc. The p1nc solutions lose stability in a secondary bifurcation near $R = 61$ (not followed here), and eventually all branches undergo a fold between $R = 36$ and $R = 24$, and turn into small amplitude branches.

Similar to the CSS case, here we also have $\langle \pi(\text{p1nc}) \rangle > \langle \pi(\text{FSS}) \rangle$ i.e., the patterned states yield a higher (average) profit than the flat states ³. In (c,d) we compare the FSS branch with the FCSS branch. Besides again showing that the fold of the FCSS is at much lower R , and hence the socially controlled system supports a uniform vegetation down to much lower R , this also illustrates that, at given R , $\langle P \rangle$ and $\langle v \rangle$ are significantly higher on the FCSS branch. Finally, (24) has the trivial branch $(v, w) = (0, R\beta/r_w)$, which however again is of no interest to us.

2.3 Canonical paths

2.3.1 Main results

Having computed CSS branches is only half of the program outlined above; we also need to solve the time dependent problem (18) to

- given a point (v_0, w_0) and a CSS \hat{u} , determine if there exists a canonical path from (v_0, w_0) to \hat{u} ;
- compare canonical paths $t \mapsto u(t)$ (or $(v, w, E)(t)$) to different \hat{u} , i.e.: compute and compare their economic values $J(u) := J(v_0, w_0, E)$, cf. 10, to find *optimal* paths.

Assuming that the spatial mesh consists of n points, we summarize the algorithm for the first point as follows, with more details given in [GU15, Uec15]. First we compute $\Psi \in$

³although $J_{c,a}$ and $\langle \pi \rangle$ have different interpretations, in Table 2 we use $J_{c,a}$ also for $\langle \pi \rangle$, as both are actually defined by the same expression

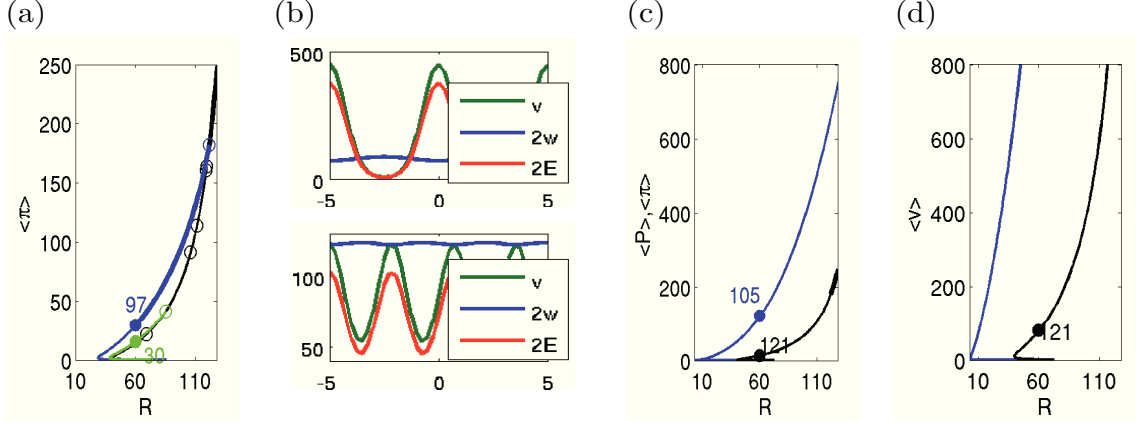


Figure 2: (a) Bifurcation diagram for the case of private optimization, where $\langle \pi \rangle$ denotes the average private profit (given by the same formula as the profit P under control); the blue branch is the primary bifurcation **p1nc**, the green is **p6nc**. (b) example solutions from (a), **p1nc/pt97** (top) and **p1nc/pt30** (bottom). (c,d) comparison of the flat states without control (black) with the OC case (blue).

$\mathbb{R}^{2n \times 4n}$ corresponding to the unstable eigenspace of \hat{u} such that the right BC $u(T) \in E_s(\hat{u})$ is equivalent to $\Psi(u(T) - \hat{u}) = 0$. Then, to solve (18) we use a modification **mtom** of the two-point BVP solver TOM [MT04], which allows to handle systems of the form $M \frac{d}{dt} u = -G(u)$, where $M \in \mathbb{R}^{4n \times 4n}$ is the mass matrix arising in the FEM discretization of (6). A crucial step in solving (nonlinear) BVPs is a good initial guess for a solution $t \mapsto u(t)$, and we combine **mtom** with a continuation algorithm in the initial states, again see [GU15, §2.1] for further discussion, and [Uec15] for implementation details.

For the second point we note that for a CSS \hat{u} we simply have $J(\hat{u}) = J_{c,a}(\hat{u})/\rho$. Given a canonical path $u(t)$ that converges to a CSS \hat{u} , and a final time T , we may then approximate

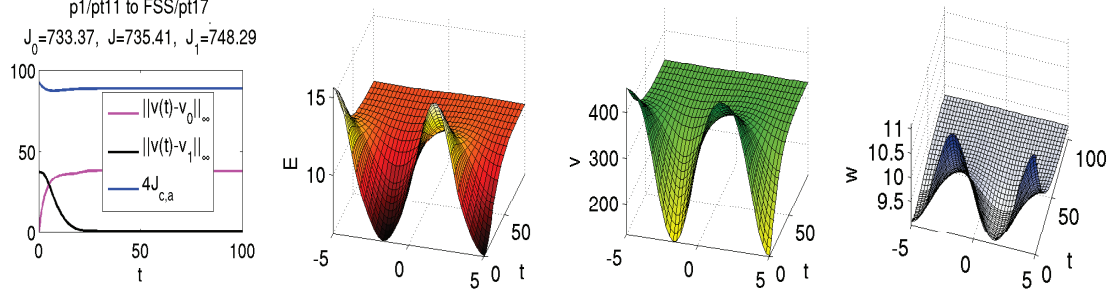
$$J(v_0, w_0, E) = \int_0^T e^{-\rho t} J_{c,a}(v(t, \cdot), E(t, \cdot)) dt + \frac{e^{-\rho T}}{\rho} J_{c,a}(\hat{u}). \quad (25)$$

In principle, given $\hat{u} = (\hat{v}, \hat{w}, \hat{\lambda}, \hat{\mu})$ with $d(\hat{u}) = 0$ we could choose any (v_0, w_0) in a neighborhood of (\hat{v}, \hat{w}) (or globally, if \hat{u} is a globally stable OSS) and aim to find a canonical paths from (v_0, w_0) to \hat{u} . However, the philosophy of our simulations rather is to start at the state values of some CSS, and see if we can find canonical paths to some other CSS which give a higher J . We discuss such canonical paths in decreasing R , starting with $R = 26$ in Fig. 3, and postponing the situation at $R = 28$ to §2.3.2.

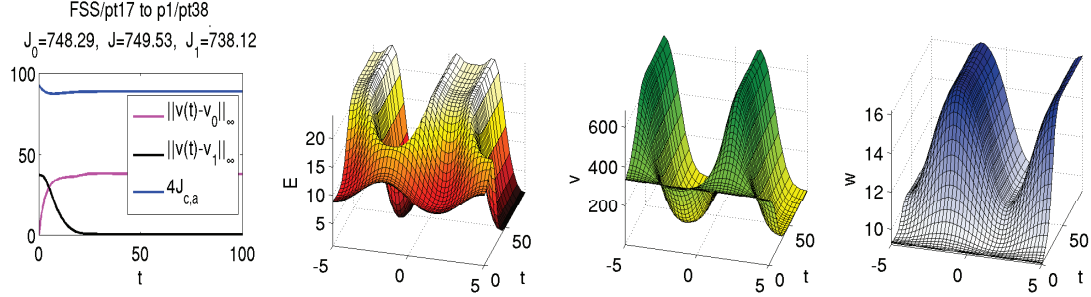
Remark 2.2. a) Note again, that our discussion is based on the primary bifurcations in R from the FCSS in Fig. 1, which misses a branch of unimodal CSS, cf. Remark 2.1 and §2.5.2. b) Although only the state values (v_0, w_0) are fixed as initial conditions for canonical paths as connecting orbits, in order not to clutter notations and language we write, e.g., $u_{\text{FCSS} \rightarrow \text{PS}}$ for a connecting orbit starting at the state values of \hat{u}_{FCSS} and connecting to \hat{u}_{PS} .]

$R = 26$. At $R = 26$ we have two CSS with $d(\hat{u}) = 0$, namely \hat{u}_{FCSS} given by FSS/pt17, and \hat{u}_{PS} given by p1/pt38. Figure 3 shows two canonical paths to these CSS. (a) shows $\|v(t) - v_0\|_\infty$ and $\|v(t) - v_1\|_\infty$ for the path from the “intermediate” patterned CSS \hat{u}_{PSI} given by p1/pt11 to \hat{u}_{FCSS} . This indicates that and how fast the canonical path leaves the initial (v_0, w_0) and approaches the goal $(v_1, w_1) = (\hat{v}, \hat{w})$ (the differences in the second component $\|w(t) - w_*\|_\infty$ are always smaller). Moreover we plot $4J_{c,a}(t)$, illustrating that $J_{c,a}(t)$ does not vary much along the canonical path. However, the differences may accumulate.

(a) Path from \hat{u}_{PSI} to \hat{u}_{FCSS} : diagnostics, control E , vegetation v and water w .



(b) Path from \hat{u}_{PSI} to \hat{u}_{PS} : diagnostics, control E , vegetation v and water w .



(c) Co-state paths from PSI to FCSS (left), and from FCSS to PS (right)

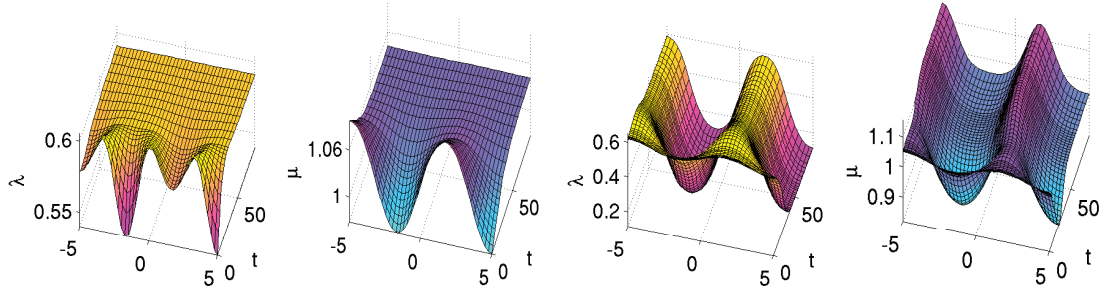


Figure 3: $R = 26$. (a) convergence behavior, the current value profit, and obtained objective values for the canonical paths from p1/pt11 to the FCSS (left), and E, v, w on the path; (b) the same for the canonical path from the FCSS to p1/pt38. (c) co-state paths from (a),(b).

The values of the solutions are as follows. We readily have

$$J(\hat{u}_{\text{PSI}}) = 733.37 < J(\hat{u}_{\text{PS}}) = 738.12 < J(\hat{u}_{\text{FCSS}}) = 748.29, \quad (26)$$

and for the paths $u_{\text{PSI} \rightarrow \text{FCSS}}$ (a,b), $u_{\text{FCSS} \rightarrow \text{PS}}$ (c), and $u_{\text{PSI} \rightarrow \text{PS}}$ (not shown) we obtain

$$J(u_{\text{PSI} \rightarrow \text{FCSS}}) = 735.51, \quad J(u_{\text{PSI} \rightarrow \text{PS}}) = 744.28, \quad \text{and} \quad J(u_{\text{FCSS} \rightarrow \text{PS}}) = 749.53. \quad (27)$$

The result for $J(u_{\text{PSI} \rightarrow \text{FCSS}})$ seems natural, as controlling the system to a CSS with a higher value should increase J . However, the results for $J(u_{\text{PSI} \rightarrow \text{PS}})$ and $J(u_{\text{FCSS} \rightarrow \text{PS}})$ may at first seem counter-intuitive. In $u_{\text{FCSS} \rightarrow \text{PS}}$ we go to a CSS with a smaller value, but the transients yield a higher profit for the path. In particular, this shows that *a CSS which maximizes J amongst all CSS is not necessarily optimal*. Similarly, although \hat{u}_{PS} as a CSS has a lower value than \hat{u}_{FCSS} , starting at \hat{u}_{PSI} it is advantageous to go to \hat{u}_{PS} rather than to \hat{u}_{FCSS} .

Due to folds in the continuation in the initial states, again see [GU15] for details, we could not compute a path from \hat{u}_{PS} to \hat{u}_{FCSS} . Thus we conclude that such paths do not exist, and (tentatively, see Remark 2.2) classify \hat{u}_{PS} as an at least locally stable POSS, with \hat{u}_{FCSS} and \hat{u}_{PSI} in its domain of attraction.

The control to go from \hat{u}_{PSI} to \hat{u}_{FCSS} in (b) is intuitively clear: Increase/decrease E near the maxima/minima of v_0 . Going from \hat{u}_{FCSS} to \hat{u}_{PS} in (c) warrants a bit more discussion: For a short transient, E is reduced around the locations $x_2 = -5$ and $x_4 = 5/3$ of the maxima of \hat{u}_{PS} . This is enough to give an increase of v around $x_{2,4}$. However, under the given conditions this does not decrease soil water near $x_{2,4}$, i.e., the increased infiltration at larger v dominates the higher uptake by plants. After this transient, E increases near $x_{2,4}$, thus producing the higher J ; see also the discussion of Fig. 4 below. As the behavior of E follows from (6e), i.e., $E = \left(\frac{(p-\lambda)(1-\alpha)}{c}\right)^{1/\alpha} v$ for illustration we also plot λ, μ for the paths in (a), (b) in Fig. 3(c).

(a) diagnostics

(b) variables on canonical path

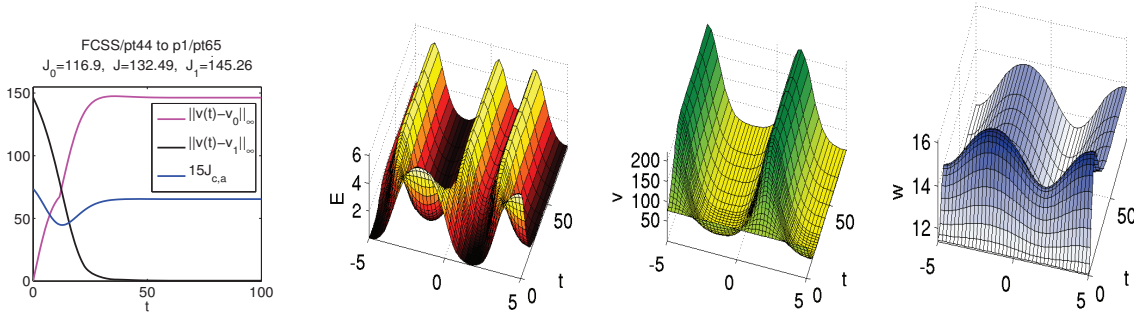


Figure 4: The canonical path from FCSS to PS at $R = 10$.

Smaller R . For $R < R_c \approx 21.5$, in Fig.1 the only CSS with the SPP is the patterned state $\hat{u}_{\text{PS}}(R)$. In Fig. 4 we focus on the case $R=10$, and here only remark that the results are qualitatively similar for all $R_{\min} < R < R_c$. We show the canonical path from the FCSS to the PCSS, where now the strategy to reach a patterned state already indicated in Fig3(c) becomes more prominent. Up to $t \approx 10$, E is reduced around $x_2 = -5$ and $x_4 = 5/3$. Conversely, E is initially increased near the minima $x_1 = -5/3$ and $x_3 = 5$ of \hat{v} , leading to a decrease of v and an increase of w near $x_{1,3}$. On the other hand, due to diffusion of w the increase of v near $x_{2,4}$ does *not* lead to a decrease of w compared to the FCSS w_0 . Instead w increases significantly *everywhere*. After this transient the harvesting effort E is increased near $x_{2,4}$, leading to an overall quick convergence of $u(t)$ to the PCSS \hat{u} .

Thus, the main point for the strategy to go from \hat{u}_{FCSS} to \hat{u}_{PS} is to initially introduce a spatial variation (of the right wavelength) into E , which yields maxima of v at the minima of this initial E , but then to rather quickly switch to the harvesting on the slopes of the generated maxima of v . The canonical path shows precisely how to do this. Also note (blue curve in (Fig. 4a)) that the initial harvesting briefly yields a higher $J_{c,a}$ than $J_{c,a}(\hat{u}_{\text{PS}})$ but in the transition $4 < t < 25$, say, $J_{c,a}(t)$ is significantly below $J_{c,a}(\hat{u}_{\text{PS}})$.

For the values we have

$$J(\hat{u}_{\text{FCSS}}) = 116.9 < J(u_{\text{FCSS} \rightarrow \text{PS}}) = 132.49 < J(\hat{u}_{\text{PS}}) = 145.26. \quad (28)$$

Thus, again tentatively, see Remark 2.2, and in particular (32) below, we classify \hat{u}_{PS} at $R = 10$ as a POSS, with \hat{u}_{FCSS} in its domain of attraction. For completeness we remark that at $R = 20$ we have

$$J(\hat{u}_{\text{FCSS}}) = 455.31, J(\hat{u}_{\text{PS}}) = 480.88, \text{ and } J(u_{\text{FCSS} \rightarrow \text{PS}}) = 474.57. \quad (29)$$

2.3.2 A patterned Skiba point

In ODE OC applications, if there are several locally stable OSS, then often an important issue is to identify their domains of attractions. These are separated by so called threshold or Skiba-points (if $N = 1$) or Skiba-manifolds (if $N > 1$) [Ski78, GCF⁺08, KW10]. Roughly

(a) A Skiba at $\alpha \approx 0.9$ (b) Paths of (almost) equal values to the FCSS and the upper PCSS.

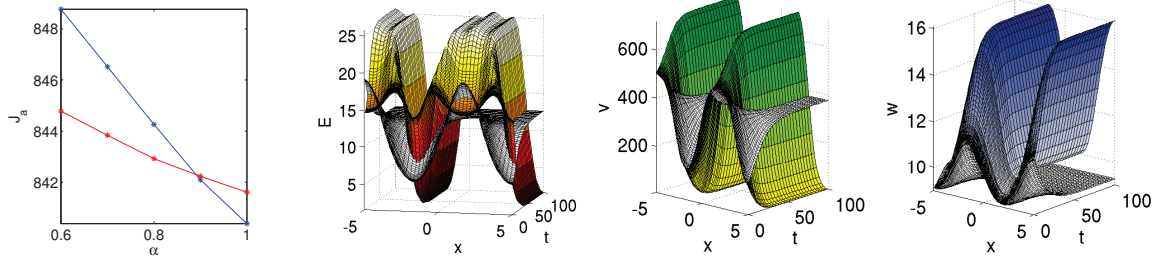


Figure 5: In (a), the blue and red lines gives J for the canonical paths $u_{\rightarrow \text{FCSS}}$ and $u_{\rightarrow \text{PS}}$ from $(v, w)_\alpha(0) := \alpha(v, w)_{\text{PS}} + (1 - \alpha)(v, w)_{\text{FCSS}}$ to FCSS/pt13 and to p1/pt34, respectively. In (b), the white surfaces are for $u_{\rightarrow \text{FCSS}}$ and the colored ones for $u_{\rightarrow \text{PS}}$.

speaking, these are (consist of) initial states from which there are more than one optimal paths *with the same value, but connecting to different CSS*. In PDE applications, even under spatial discretization with moderate nN , Skiba manifolds should be expected to become very complicated objects.

In Fig. 5 we just given one example of a patterned Skiba point “between” \hat{u}_{PS} given by p1/pt34 and \hat{u}_{FCSS} given by FCSS/pt13, at $R = 28$, where \hat{u}_{PS} and \hat{u}_{FCSS} are the two possible targets for canonical paths. The blue and red lines in (a) gives J for the canonical paths as indicated. The lines intersect near $\alpha \approx 0.9$, giving the same value J . Hence, while the two paths are completely different, they both are equally optimal, and for illustration (b) shows the two paths for $\alpha = 0.9$, where $|J_{\rightarrow \text{FCSS}} - J_{\rightarrow \text{PS}}| < 0.08$.

2.4 2D results

The basic mechanisms of pattern formation in reaction–diffusion models can usually be studied in 1D, but for quantitative results for vegetation–water ecosystem models one should also consider the more pertinent 2D situation, and clearly the same applies to the OC system. Even though we do not expect qualitatively different results from the 1D case, here we give a short overview over 2D PCSS and the associated canonical paths.

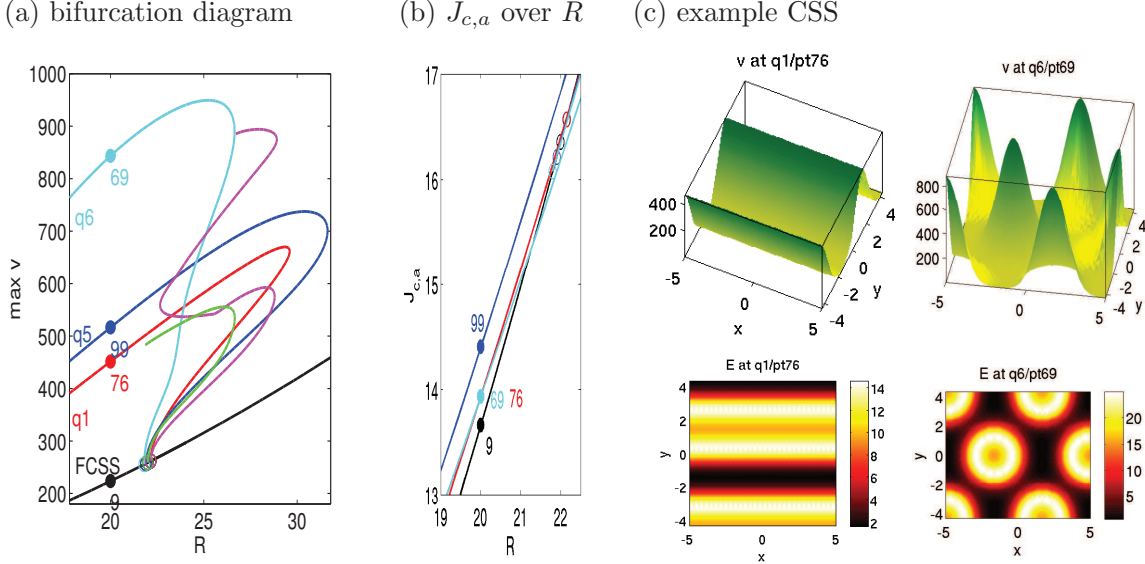


Figure 6: Partial bifurcation diagram and example plots of CSS in 2D.

The first question concerns the second spatial length, now called y -direction. For classical Turing bifurcations, typically stripes and/or hexagonal spots are the most stable bifurcating 2D patterns, see [UW14] and the references therein for discussion, and thus by analogy here we choose the domain $\Omega = (-L, L) \times (-\sqrt{3}L/2, \sqrt{3}L/2)$ with $L = 5$ as in 1D. Figure 6(a) shows five branches bifurcating from the FCSS. It turns out, that the 1D branch p1 actually comes out of the 5th bifurcation point in 2D, and is therefore called q5 now, while the first branch q1 corresponds to horizontal stripes, see (c). Thus, $L = 5$, chosen for simplicity, does not capture the first instability in 1D. However, the first bifurcation points are very close together; moreover, upon continuation to low R the q5 branch still yields the highest $J_{c,a}$, see (b).

The sixth branch q6 is a hexagon branch. Similar to q5, both q1 and q6 have the SPP after their first folds. The other branches are other types of stripes or spots, for instance “squares”, but none of these have the SPP. All branches exhibit some secondary bifurcations, not shown here, and to not overload the bifurcation diagram we only plot the starting segments of q2 (green) and q3 (magenta).

At, for instance, $R = 20$ we now have 3 possible targets for canonical paths: \hat{u}_{hs} (horizontal stripes) from q1, \hat{u}_{hex} (hexagons) from q6, and \hat{u}_{vs} (vertical stripes) from q5, already discussed in 1D as p1. It turns out that we can reach each of these from the FCSS, with $J(\hat{u}_{\text{FCSS}}) =$

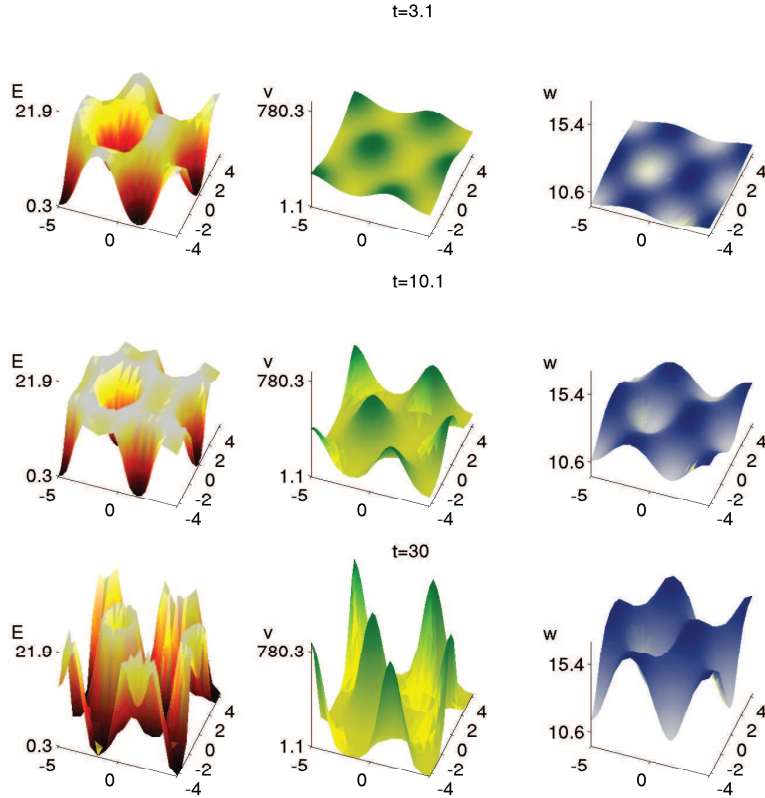


Figure 7: Snapshots of E and (v, w) on the canonical path from the FCSS to the hexagons. The states v, w both go directly into their ultimate hex pattern, which then only grows, while E shows a switching analogously to the 1D case.

455.31, cf. (29), and similarly $J(\hat{u}_{vs}) = 480.88$ and $\hat{u}_{\text{FCSS} \rightarrow vs} = 474.56$ as in 1D (since these values are normalized by $|\Omega|$). For the path to \hat{u}_{hs} with $J(\hat{u}_{hs}) = 464.33$ we obtain $J = 464.91$, and the path to \hat{u}_{hex} with $J(\hat{u}_{hex}) = 464.33 = J(\hat{u}_{hs})$ (up to 2 digits) yields $J = 467.38$. Thus we again have $V(\hat{u}_{\text{FCSS}}) = 474.6$. The strategies for these paths are the natural extensions of the 1D case: given a target PCSS \hat{u} , initially E has minima at the maxima of \hat{v} , but after a rather short transient during which $v(t, \cdot)$ develops maxima at the right places, E changes to harvesting in the neighborhood of these maxima. Movies of these paths can be found at [Uec14], and in Fig. 7 we present some snapshots. We could not compute canonical paths from any of the PCSS to any other PCSS, with the continuation typically failing due to a sequence of folds. Thus we strongly expect all three PCSS to be locally stable POSS.

2.5 Remarks on further parameter dependence

So far we varied the rainfall R as our external bifurcation parameter. Similarly, we could vary some other of the physical parameters $g, \eta, \dots, d_{1,2}$ (first six rows of Table 1), and in most cases may expect bifurcations to patterned CSS.

Maybe even more interesting from an application point of view is the dependence on the economic parameters ρ, c, p and α (discount rate, cost for harvesting, price of harvest, and elasticity), as these may vary strongly with economic circumstances. Moreover, varying a second parameter often also gives bifurcations to branches which were missed upon contin-

uation of just the primary parameter, and these may play an important role in the overall structure of the solution set; this does happen here, see §2.5.2 below.

2.5.1 Experiments with the discount rate ρ

In Fig.8 we illustrate the dependence of the PCSS on the p1 branch from Fig. 1 on ρ , at fixed $R = 10$, cf. also Fig. 4. Panel (a) shows the bifurcation diagram; to obtain the blue and black branches we continued the points p1/pt65 and FCSS/pt44 from $\rho = 0.03$ down to $\rho = 0.005$, reset counters, renamed p1 to r1, and continued to larger ρ again. Both, the FCSS and the r1 branches then show some folds at $\rho \approx 0.185$ and $\rho \approx 0.325$, respectively. More importantly, the r1 branch has the SPP for small ρ , but loses it at $\rho \approx 0.032$ to another PCSS branch s1. Solutions on s1 have maxima of different heights in v , see (b), and have the SPP only up to the fold at $\rho = \rho_f \approx 0.046$. Moreover, there are further bifurcations from the FCSS branch to PCSS branches, but none of these has the SPP.

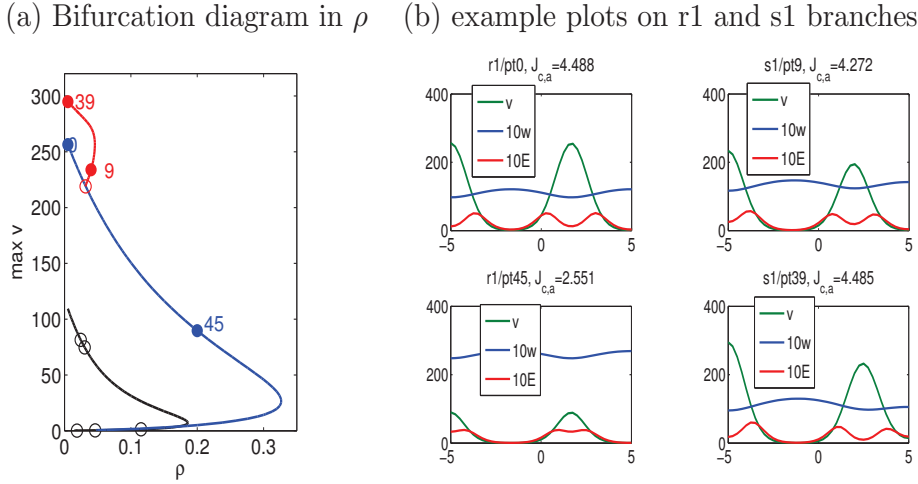


Figure 8: Bifurcations when varying the discount rate ρ at $R = 10$. The blue branch (which at $\rho = 0.03$ corresponds to Fig. 4) loses the SPP at $\rho \approx 0.032$, where the red s1-branch bifurcates, which has the SPP up to its fold.

With \hat{u}_{PS} given by s1/pt9 ($\rho = 0.04$), the control to go from the FCSS to \hat{u} shows a similar switching strategy as, e.g., in Fig. 4. The values are

$$J(\hat{u}_{FCSS}) = 82.5, \quad J(u_{FCSS \rightarrow PS}) = 92.8, \quad J(\hat{u}_{PS}) = 106.8, \quad (30)$$

which are more or less comparable to Fig. 4 (with $\rho = 0.03$). On the other hand, for the canonical path from the FCSS to r1/pt0 at $\rho = 0.005$ we obtain

$$J(\hat{u}_{FCSS}) = 774.9, \quad J(u_{FCSS \rightarrow PS}) = 892.2, \quad J(\hat{u}_{PS}) = 897.7. \quad (31)$$

Additional to the larger total values due to the smaller discount rate, compared to Fig. 4 the canonical path to \hat{u}_{PS} now has almost the same value as \hat{u}_{PS} itself. This illustrates that at low ρ the transients have less influence, as expected.

For $\rho > \rho_f$ none of the CSS on the branches that are shown in Fig. 8, or that can be obtained from the shown bifurcation points, have the SPP. This does not mean that PCSS with the SPP do not exist in this parameter regime, but rather that they must be obtained by continuation and bifurcation in some other way, cf. Remark 2.1 and §2.5.2.

2.5.2 Dependence on the price p , and the unimodal branch

In Fig. 9(a) we illustrate the dependence of the FCSS and p1 branches on the price p , with fixed $R = 10$, starting at $p = 1.1$ with p1/pt65 and FCSS/pt44 from Fig. 1, respectively. Naturally, the values decrease as p decreases, and not surprisingly p1 bifurcates from the FSS branch at some $p_c \approx 0.55$. Next, as an additional benefit we find the “unimodal” branch p0, which bifurcates from the FCSS branch near $p=0.5$, and which yields a higher $J_{c,a}$ than p1.

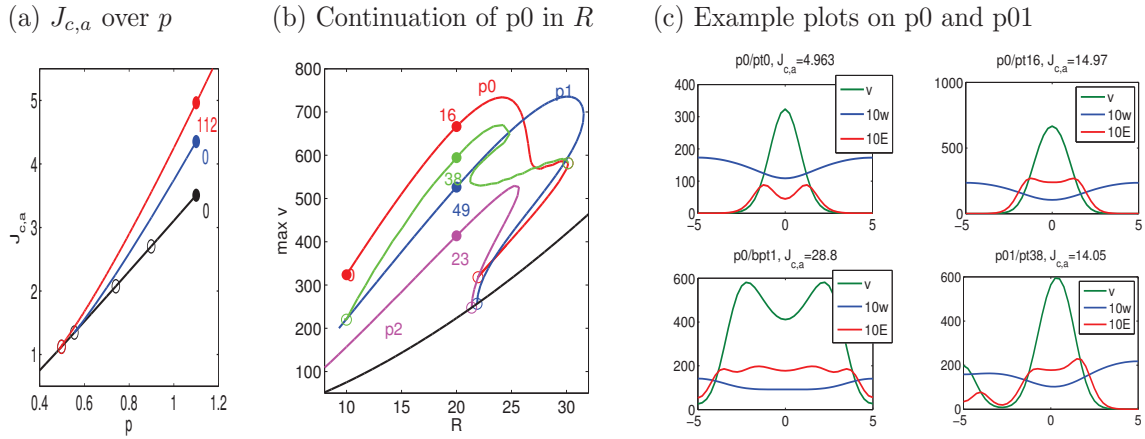


Figure 9: (a) branches FCSS (black), p1 (blue), and p0 (red) over p , $R = 10$ fixed. (b) Continuation in R of new branch p0 found in (a), and bifurcating branch p01 (green), together with known branches FSS (black) and p2 from Fig. 1. Example plots in (c).

Thus, in a next step we continue p0 to $p = 1.1$ and then switch back to continuation in R , with $p = 1.1$ fixed, i.e., p0/pt0 in (b)-(c) is pt112 from (a). It turns out that the p0 branch has the SPP up the fold at $R_f \approx 30.15$, and slightly below the fold there is a bifurcation point to the green branch. This contains some “skewed” solutions, and connects p0 and p1. Ultimately, p0 connects back to p2 from Fig. 1 at low amplitude near $R = 21.1$. Thus, we could also have found p0 by following secondary bifurcations in Fig. 1. The values pertinent for the canonical path from FCSS/pt44 to p0/pt0 are

$$J(\hat{u}_{\text{FCSS}}) = 116.9 \text{ (as in (28))}, \quad J(u_{\text{FCSS} \rightarrow \text{P0}}) = 145.11, \quad J(\hat{u}_{\text{P0}}) = 165.42, \quad (32)$$

which shows that the path to p0 dominates the path to p1 from Fig. 4. Thus, the point FCSS/pt44 is in the domain of attraction of p0, and not of p1.

On the other hand, we could not find canonical paths from p1/pt65 to p0/pt0 (or vice versa). Therefore p1/pt65 can still be classified as an at least locally stable POSS, and similarly, p0/pt0 is *only locally stable*, since it does not attract p1/pt65. Next one could

compute a number of Skiba-points (cf. §2.3.2) “between” p_0 and p_1 to roughly characterize the respective domains of attraction, but here we refrain from this.

Finally, despite trying some further combinations of continuations/bifurcations and also suitable direct initial guesses followed by a Newton loop, we could not find a “half”-modal branch in the parameter regions studied so far, i.e., a branch on which solutions are monotonous in v . Thus, it appears that such “long wave” PCSS, i.e., with period 20, do not exist in these parameter regions.

3 Summary and discussion

Our numerical approach for spatially distributed optimal control problems may yield rich results, if applied carefully, in the following sense. First, the canonical system may have many steady states, and it is in general not clear how to find all *relevant* CSS, and which of the CSS have the SPP and hence are suitable targets for canonical paths, and second it needs to be checked which CSS ultimately belong to optimal paths.

On the other hand, the value J of the CSS can easily be calculated in parallel with the bifurcation diagram of the CSS, allowing to identify which CSS maximize J amongst all CSS. Compared to the computation of canonical paths (or direct methods for the optimization problem (3)), this first step is relatively cheap numerically, but (together with the SPP) typically still gives a strong indication for optimal CSS.

The computation of canonical paths is a connecting orbits problem, and in particular in two spatial dimensions this may become numerically expensive. In practice we found our two-step approach to be reasonably fast for up to 5000 degrees of freedom of u at fixed time, e.g., for our vegetation model 1250 spatial discretization points and 4 components, and up to 100 temporal discretization points; up to such values a continuation step in the calculation of a canonical path takes up to a minute on a desktop computer (Intel i7, 2.3 GHz), such that a typical canonical path is computed in about 5 continuation steps in at most 5 minutes, and often much more quickly. In 1D, with $n = 50$, say, typical canonical paths are computed in a few seconds.

Here we applied our method exemplarily to the optimal control model from [BX10], and for this we again summarize our main results as follows, cf. also **(a)**–**(d)** in the Introduction:

- (i) Compared to the case of private optimization, we have CSS (both flat and patterned) for significantly lower rainfall values R , and the whole Turing (like) bifurcation scenario is shifted to lower R . This is important for welfare as it means a much increased robustness of vegetation (and hence harvest) with respect to low rainfall. Moreover, at a given R the social control gives a significantly (almost ten times) higher J for steady states than private optimization; see, e.g., Table 2, bottom center, and Fig. 2(c), for numerical values.
- (ii) At low R , some PCSS yield a higher J than the FCSS, and some of these PCSS are locally stable POSS.
- (iii) The optimal controls to reach such a POSS \hat{u} from a FCSS follow some general rules: first decrease the harvesting effort E at the location of the maxima of the desired POSS,

then start harvesting near (but not at) the maxima of the POSS, as determined by E from the POSS. The increase in welfare by controlling the system from a FCSS to a POSS can be up to 40%, see (32). See also, e.g., (27), (28), (29), and the values given in §2.4 for further numerical values.

- (iv) The co-state (or shadow price) λ computed for an optimal path can be interpreted as an optimal tax for private optimization, see Remark 1.4.

The points (ii) and (iii) emphasize that resource management rules in systems with multiple CSS may need to take several of these into account, as also illustrated by the Skiba point computations in §2.3.2. We strongly expect similar results about POSS in other spatially distributed optimal control problems for (Turing like) systems of PDE. Thus we hope that our numerical approach is a valuable tool to study the basic behavior of spatially distributed optimal control models with the states fulfilling a reaction diffusion system.

References

- [AAC11] S. Anița, V. Arnăutu, and V. Capasso. *An introduction to optimal control problems in life sciences and economics*. Birkhäuser/Springer, New York, 2011.
- [ACKLT13] S. Anița, V. Capasso, H. Kunze, and D. La Torre. Optimal control and long-run dynamics for a spatial economic growth model with physical capital accumulation and pollution diffusion. *Appl. Math. Lett.*, 26(8):908–912, 2013.
- [ADS14] N. Apreutesei, G. Dimitriu, and R. Strugariu. An optimal control problem for a two-prey and one-predator model with diffusion. *Comput. Math. Appl.*, 67(12):2127–2143, 2014.
- [BEGX13] W.A. Brock, G. Engström, D. Grass, and A. Xepapadeas. Energy balance climate models and general equilibrium optimal mitigation policies. *Journal of Economic Dynamics and Control*, 37(12):2371–2396, 2013.
- [BPS01] W.J. Beyn, Th. Pampel, and W. Semmler. Dynamic optimization and Skiba sets in economic examples. *Optimal Control Applications and Methods*, 22(5–6):251–280, 2001.
- [BX08] W.A. Brock and A. Xepapadeas. Diffusion-induced instability and pattern formation in infinite horizon recursive optimal control. *Journal of Economic Dynamics and Control*, 32(9):2745–2787, 2008.
- [BX10] W. Brock and A. Xepapadeas. Pattern formation, spatial externalities and regulation in coupled economic–ecological systems. *Journal of Environmental Economics and Management*, 59(2):149–164, 2010.
- [Cla90] C. W. Clark. *Mathematical bioeconomics*. John Wiley & Sons, Inc., New York, second edition, 1990. The optimal management of renewable resources.
- [CPB12] C. Camacho and A. Pérez-Barahona. Land use dynamics and the environment. Documents de travail du Centre d’Economie de la Sorbonne, 2012.
- [DBC⁺08] V. Deblauwe, N. Barbier, P. Couteron, P. Lejeune, and J. Bogaert. The global biogeography of semi-arid periodic vegetation patterns. *Global Ecol. Biogeogr.*, 17:715–723, 2008.
- [DL09] W. Ding and S. Lenhart. Optimal harvesting of a spatially explicit fishery model. *Natural Resource Modeling*, 22(2):173–211, 2009.

- [DRUW14] T. Dohnal, J. Rademacher, H. Uecker, and D. Wetzel. pde2path 2.0. In H. Ecker, A. Steindl, and S. Jakubek, editors, *ENOC 2014 - Proceedings of 8th European Nonlinear Dynamics Conference*, ISBN: 978-3-200-03433-4, 2014.
- [GCF⁺08] D. Grass, J.P. Caulkins, G. Feichtinger, G. Tragler, and D.A. Behrens. *Optimal Control of Nonlinear Processes: With Applications in Drugs, Corruption, and Terror*. Springer Verlag, 2008.
- [Gra15] D. Grass. From 0D to 1D spatial models using OCMat. Technical report, ORCOS, 2015.
- [GRS14] K. Gowda, H. Riecke, and M. Silber. Transitions between patterned states in vegetation models for semiarid ecosystems. *PRE*, 89:022701, 2014.
- [GU15] D. Grass and H. Uecker. Optimal management and spatial patterns in a distributed shallow lake model. Preprint, 2015.
- [HRvdB⁺01] R. HillerisLambers, M.G. Rietkerk, F. van den Bosch, H.H.T. Prins, and H. de Kroon. Vegetation pattern formation in semi-arid grazing systems. *Ecology*, 82:50–61, 2001.
- [KW10] T. Kiseleva and F.O.O. Wagener. Bifurcations of optimal vector fields in the shallow lake system. *Journal of Economic Dynamics and Control*, 34(5):825–843, 2010.
- [KXL15] M. R. Kelley, Y. Xing, and S. M. Lenhart. Optimal fish harvesting for a population modeled by a nonlinear parabolic partial differential equation. *Natural Resource Modeling*, DOI 10.1111/nrm.12073, 2015.
- [LM01] S. M. Lenhart and J. A. Montero. Optimal control of harvesting in a parabolic system modeling two subpopulations. *Math. Models Methods Appl. Sci.*, 11(7):1129–1141, 2001.
- [LW07] S. Lenhart and J. Workman. *Optimal Control Applied to Biological Models*. Chapman Hall, 2007.
- [MT04] F. Mazzia and D. Trigiante. A hybrid mesh selection strategy based on conditioning for boundary value ODE problems. *Numerical Algorithms*, 36(2):169–187, 2004.
- [Mur89] J. D. Murray. *Mathematical Biology*. Springer, Berlin, 1989.
- [Neu03] M. G. Neubert. Marine reserves and optimal harvesting. *Ecology Letters*, 6(9):843–849, 2003.
- [NPS11] I. Neitzel, U. Prüfert, and Th. Slawig. A smooth regularization of the projection formula for constrained parabolic optimal control problems. *Numer. Funct. Anal. Optim.*, 32(12):1283–1315, 2011.
- [QB12] M.F. Quaas and S. Baumgärtner. Optimal grazing management rules in semi-arid rangelands with uncertain rainfall. *Natural Resource Modeling*, 25(2):364–387, 2012.
- [RDdRvdK04] M.G. Rietkerk, S.C. Dekker, P.C. de Ruiter, and J. van de Koppel. Self-organized patchiness and catastrophic shifts in ecosystems. *Science*, 305:1926–1929, 2004.
- [RZ99a] J. P. Raymond and H. Zidani. Hamiltonian Pontryagin’s principles for control problems governed by semilinear parabolic equations. *Appl. Math. Optim.*, 39(2):143–177, 1999.
- [RZ99b] J. P. Raymond and H. Zidani. Pontryagin’s principle for time-optimal problems. *J. Optim. Theory Appl.*, 101(2):375–402, 1999.
- [SBB⁺09] M. Scheffer, J. Bascompte, W. A. Brock, V. Brovkin, St. R. Carpenter, V. Dakos, H. Held, E. H. van Nes, M. Rietkerk, and G. Sugihara. Early-warning signals for critical transitions. *Nature*, 461:53–59, 2009.

- [Ski78] A. K. Skiba. Optimal growth with a convex-concave production function. *Econometrica*, 46(3):527–539, 1978.
- [SZvHM01] M. Shachak, Y. Zarmi, J. von Hardenberg, and E. Meron. Diversity of vegetation patterns and desertification. *PRL*, 87, 2001.
- [Trö10] Fredi Tröltzsch. *Optimal control of partial differential equations*, volume 112 of *Graduate Studies in Mathematics*. American Mathematical Society, Providence, RI, 2010.
- [Uec14] H. Uecker. pde2path, www.staff.uni-oldenburg.de/hannes.uecker/pde2path, 2014.
- [Uec15] H. Uecker. The pde2path add-on library p2poc for solving o infinite time-horizon spatially distributed optimal control problems - Quickstart Guide. Preprint, 2015.
- [UW14] H. Uecker and D. Wetzel. Numerical results for snaking of patterns over patterns in some 2D Selkov-Schnakenberg Reaction-Diffusion systems. *SIADS*, 13-1:94–128, 2014.
- [UWR14] H. Uecker, D. Wetzel, and J. Rademacher. pde2path – a Matlab package for continuation and bifurcation in 2D elliptic systems. *NMTMA*, 7:58–106, 2014.
- [Xep10] A. Xepapadeas. The spatial dimension in environmental and resource economics. *Environment and Development Economics*, doi:10.1017/S1355770X10000355, 2010.
- [ZKY⁺13] Y. Zelnik, S. Kinast, H. Yizhaq, G. Bel, and E. Meron. Regime shifts in models of dryland vegetation. *Philos. Trans. R. Soc. Lond. Ser. A Math. Phys. Eng. Sci.*, 371(2004), 2013.